

Acousto-optic k -space Filtering of Optical Beams

Konstantin B. Yushkov ^a

National University of Science and Technology “MISIS”, 4 Leninsky Prospekt, Moscow 119049, Russia

Keywords: Acousto-optics, Tunable Filter, Spatial Filter, Phase Imaging, Optical Trapping.

Abstract: Acousto-optic tunable filters (AOTFs) can be used for spatial filtering of optical beams. A noncollinear AOTF has a tunable ring-shaped transfer function determined by geometry of the refractive index surface in a uniaxial crystal. Different axially symmetric transfer functions can be synthesized using multi-frequency ultrasonic signals. In the report, theory of AOTF-based spatial filtering of optical beams is summarized. Specific transfer function of the AOTF — bandpass spatial frequency filter — enables hyperspectral phase imaging in dark-field mode using incoherent illumination. Operation of a dynamic ring-shaped optical trap based on the noncollinear AOTF is demonstrated.

1 INTRODUCTION

Acousto-optic tunable filters (AOTF) find broad applications as hyperspectral imaging devices (wide-aperture monochromators and programmable multi-window filters) in the fields of biophotonics, remote sensing, and space research (Lu and Fei, 2014; Korablev et al., 2018; Genchi et al., 2021). Besides that, AOTFs are also capable of tunable spatial filtering of optical beams. This feature has been known since 1980-ies (Balakshy, 1984), but only a few of its applications in Optics, Photonics, and Laser Physics have been reported until recently (Balakshy and Voloshinov, 2005; Balakshy and Kostyuk, 2009). In this report, fundamentals and novel applications of AOTF-based optical beam shaping are observed.

Anisotropic acousto-optic diffraction in Bragg regime is used in AOTFs. It is a three-wave mixing linear optical interaction, which is governed by the phase matching condition. Ultrasonic wave produces periodic modulation of refractive index in an interaction medium — a volume phase grating to which a reciprocal grating vector can be assigned. Efficient interaction is only possible if momentum of interacting waves is conserved. Thus, Bragg phase matching determines wavelength and angular selectivity that enables design of tunable optical filters. Interaction of finite-size optical beams is analyzed using plane wave decomposition. As the result, the acousto-optic filter can operate as a tunable k -space filter of optical beams.

^a  <https://orcid.org/0000-0001-9015-799X>



Figure 1: Noncollinear paratellurite AOTF: (a) real-size photograph; (b) acoustic field visualization: left — 0th order; right — 1st order; white rectangle — optical aperture; yellow rectangle — piezotransducer (PT).

A paratellurite (TeO_2) single crystal AOTF designed and fabricated in-house (NUST “MISIS”) is shown in Fig. 1 (a). There are two beams at the AOTF output: the 0th and the 1st diffraction orders, Fig. 1 (b). The AOTF demonstrates diffraction efficiency over 98% in the optical aperture area ($5 \times 5 \text{ mm}^2$) and homogeneity of the diffracted field intensity within 15% r.m.s.

2 FUNDAMENTALS

2.1 AOTF Transfer Function

The transfer function of a linear space-invariant optical system is defined as a transmission coefficient of the angular spectrum (Goodman, 2005). The first-order transmission coefficient of a Bragg grating is derived from plane-wave coupling-of-modes theory (Yariv and Yeh, 1984):

$$H_{ao}(k_x, k_y; F) = \frac{Q}{\sqrt{Q^2 + R^2(k_x, k_y; F)}} \times \sin \frac{\pi}{2} \sqrt{Q^2 + R^2(k_x, k_y; F)}, \quad (1)$$

where Q is the coupling coefficient and $R(k_x, k_y; F)$ is the phase mismatch depending transverse components of the wave vector k_x and k_y and ultrasound frequency F provided optical frequency λ is given.

The mismatch $R(k_x, k_y; F)$ is calculated from a 3D wave vector diagram, see Fig. 2. AOTFs are designed in uniaxial crystals using their birefringence. To obtain wide acceptance angle, which is necessary for image processing, noncritical phase matching (NPM) geometry is chosen. Angular bandwidth of NPM is directly related to curvature of the optical wave normal surface in the crystal (Yushkov, 2021; Yushkov and Naumenko, 2021). It follows from differential geometry of wave normal surfaces that two fundamental topologies of phase matching in the neighborhood of NPM points are elliptical and hyperbolic. The NPM frequency F_{npm} is a local minimum of $F(k_x, k_y)$ for the elliptical topology and the saddle point for the hyperbolic one. Topological transition between these geometries takes place only at certain direction of ultrasound, which are determined only by principal values of dielectric permittivity tensor (Yushkov and Naumenko, 2021). The vector diagram in Fig. 2 illustrates conical phase matching in a positive uniaxial crystal.

Explicit expression for $R(k_x, k_y; F)$ in a non-collinear acousto-optic diffraction geometry in uniaxial crystals can be found elsewhere (Yushkov et al., 2020a; Yushkov et al., 2020b). Figure 3 shows a typical phase matching surface in k -space ($k_x \propto \delta\theta_{12}$, $k_y \propto \delta\theta_{11}$).

Intensity transfer function

$$T_1(k_x, k_y) = |H_{ao}(k_x, k_y)|^2 \quad (2)$$

can be readily visualized in experiment. The setup for transfer function visualization is schematically shown in Fig. 4 (a). A collimated laser beam is focused onto an AOTF. An output polarizer is used to select one of the diffraction orders. The output beam is captured from a screen with a CCD. Experiment in Figs 4

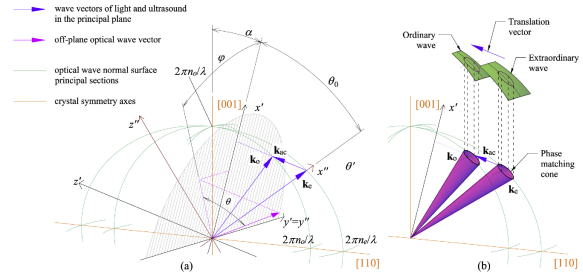


Figure 2: 3D wave vector diagram of anisotropic Bragg diffraction: (a) definition of angular coordinates for off-axial diffraction in a uniaxial crystal; (b) conical phase matching in the neighborhood of the noncritical phase matching geometry. Reproduced under Open Access Licence from (Yushkov et al., 2020a), ©2020 OSA.

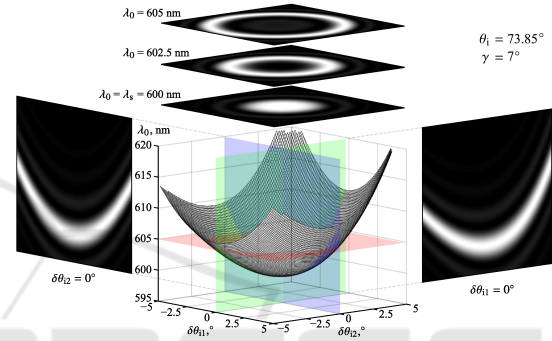


Figure 3: Zero phase mismatch surface: the case of non-collinear AOTF. Reproduced under Open Access Licence from (Gorevoy et al., 2021), ©2021 OSA.

(b)-(d) shows the transfer function T_1 measured experimentally. Paratellurite AOTF with acoustic beam orientation $\alpha = 9.06^\circ$ and $\lambda = 532$ nm laser were used, the transfer functions were measured at RF signal frequencies of 132.4, 133.0, and 133.6 MHz. The first result is a low-pass angular frequency filter with maximum transmission at $k_x = k_y = 0$ at $F \approx F_{\text{npm}} = 132.4$ MHz. The other results demonstrate a tunable bandpass filter with almost circular phase matching locus $k_x^2 + k_y^2 = \rho^2$ with $\rho^2 \propto (F - F_{\text{npm}})$. Simulations show that at low paratellurite crystal cut angles ($\alpha \lesssim 12^\circ$) the transfer function asymmetry manifests itself mainly as the shift of the transfer function center (Yushkov et al., 2020b).

2.2 Optical System Layouts

Two common optical schemes for AOTF-based optical beam shaping systems are shown in 5: the confocal one and the Fourier-transform one. For simplicity, both optical schemes in Fig. 5 are shown with unity scaling factors and equal focal lengths f of front-end and back-end optics. A general case of arbitrary focal lengths can be analyzed in the same way. Beam stops

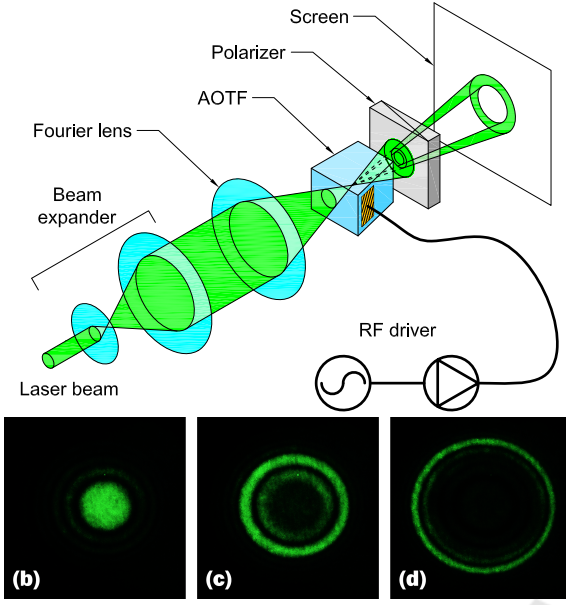


Figure 4: Visualization of AOTF transfer function: (a) experiment scheme; (b)-(d) first-order AOTF transfer functions measured at different signal frequencies.

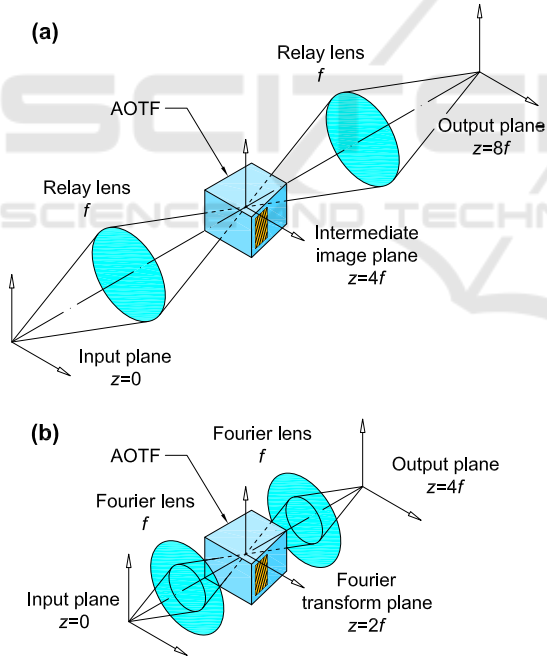


Figure 5: Two principal layouts of AOTF-based spatial filtering schemes: (a) confocal scheme; (b) Fourier-transform scheme.

to separate the diffraction orders are assumed but not plotted.

The confocal system shown in Fig. 5 (a) performs direct k -space filtering of the optical beam:

$$A_{\text{out}}(k_x, k_y) = H_{\text{ao}}(k_x, k_y) A_{\text{in}}(k_x, k_y). \quad (3)$$

In this scheme, the input field $U_{\text{in}}(x, y)$ is relayed to the AO interaction plane and its angular spectrum is unaltered. The diffracted field has the angular spectrum modified according to Eq. (3).

The confocal optical scheme is typical for low-aberration hyperspectral imaging systems (Suhre et al., 2004). Annular transfer function of the AOTF enables application of this scheme for hyperspectral imaging in dark field mode. Application of this new imaging modality for phase imaging is discussed in Sec. 3.1.

The Fourier-transform optical scheme shown in Fig. 5 (b). In this scheme, the AOTF transfer function is a complex-valued multiplier in the output field distribution:

$$U_{\text{out}}(x, y) = H_{\text{ao}}\left(\frac{x}{\lambda f}, \frac{y}{\lambda f}\right) U_{\text{in}}(x, y) \quad (4)$$

where the scaling factor between k -space and coordinate space (x, y) is λf : $x/(\lambda f) = k_x$ and $y/(\lambda f) = k_y$. Derivation of Eq. (4) simply follows from properties of optical Fourier transform performed by a lens (Goodman, 2005):

$$U_{\text{fp}}(x, y) = \frac{1}{i\lambda f} \iint_{-\infty}^{+\infty} U_{\text{in}}(x', y') \times \exp\left[-\frac{2\pi i}{\lambda f}(xx' + yy')\right] dx' dy' \quad (5)$$

is the optical field at the Fourier plane $z = 2f$ (i.e., at the AOTF input), and

$$A_{\text{fp}}(k_x, k_y) = -i\lambda f U_{\text{in}}(-\lambda f k_x, -\lambda f k_y) \quad (6)$$

is its plane wave spectrum. Equation (4) explicitly follows from applying the optical Fourier transform twice.

Fourier-transform scheme is an effective solution for laser beam shaping. Dynamic annular optical trap based on this principle is described in Sec. 3.2.

2.3 Laser Beam Shaping

Laser beam shaping is a new branch in acousto-optic instrumentation, which broadens the range of applied problems in science and engineering solved with the usage of the effect of light diffraction by ultrasound (Yushkov et al., 2018). It can extend operation rates of current beam shaping methods (Dickey, 2014) up to 100 kHz owing to fast response of AOTFs and other acousto-optic devices.

Transfer function analysis in Sec. 2.1 was made under assumption of single-frequency RF signals resulting in a periodic phase grating with unique grating vector \mathbf{k}_{ac} . A straightforward way to synthesize transfer functions with variable transmission width is

to apply multifrequency RF signals. Each monochromatic component of ultrasound will provide phase matching at its own locus of spatial frequencies resulting in broadening of the transfer function or generation of multiple independent rings. Acoustic time aperture of the AOTF, τ_{ac} , is the minimum time required to change transfer function. The time aperture is reciprocal to RF phase matching bandwidth δF .

In order to provide controllable phase relations between components of the RF signal, one can use dispersive waveform synthesis (Yushkov et al., 2019b). The ultrasonic signal $S(t)$ is calculated as the Fresnel transform (i.e., Fourier transform with quadratic spectral phase factor) of the transmission window function $W(F_k)$:

$$S(t) = \frac{1}{K} \sum_{k=1}^K W(F_k) \exp\left(\frac{\pi i F_k^2 \tau_{ac}}{\Delta F}\right) \times \exp(-2\pi i F_k t), \quad (7)$$

where ΔF is the effective FWHM signal bandwidth; the number of sampling points is determined from the Nyquist criterion, $K = 2\Delta F \tau_{ac}$; and the frequency grid centered at the frequency F_c is

$$F_k = \Delta F \frac{2k - K - 1}{K - 1} + F_c. \quad (8)$$

Equation (7) was derived to comply with the periodicity property of discrete Fourier transform. The central frequency F_c can be chosen arbitrarily that allows continuous tuning of the transmitted interval of spatial frequencies.

The signal $S(t)$ is sampled and synthesized using an RF arbitrary waveform generator (AWG). In eq. (7) it was assumed that two conditions are met to provide stationary AOTF transmission with minimized distortions:

1. RF signal period equals the AOTF time aperture τ_{ac} ;
2. the transmission window satisfies the uncertainty relation for chirped pulses (Yushkov et al., 2021b).

The dispersive waveform synthesis method enables such output modes as flat-top laser beam shaping and generation of bottle laser beams with variable diameter and wall thickness (Yushkov et al., 2021a). The examples of Gaussian laser beam shaping are shown in Fig. 6. Panels (a) and (c) were obtained with single-frequency RF signals corresponding to Fig. 4; panels (b) and (d) were obtained with multi-frequency RF signals synthesized according to (7).

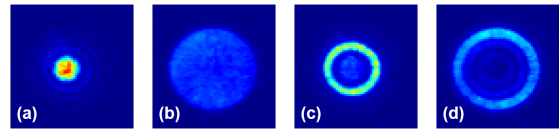


Figure 6: Laser beam shaping with a noncollinear AOTF: (a) low-pass spatial filtering; (b) flat-top beam shaping; (c) band-pass spatial filtering; (d) bottle beam shaping. Reproduced from (Yushkov et al., 2021a), ©2021 SPIE–OSA.

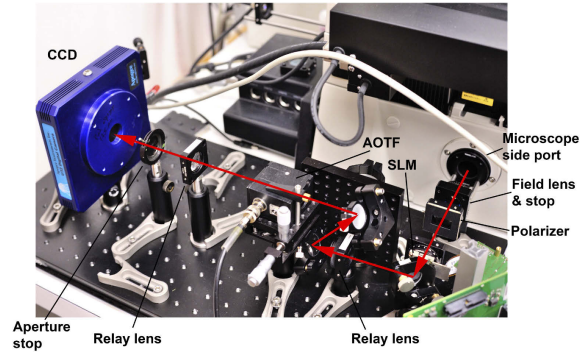


Figure 7: Experimental setup for hyperspectral phase imaging based on AOTF operation in dark-field mode: red arrows — optical path. Reproduced under Open Access Licence from (Yushkov et al., 2020a), ©2020 OSA.

3 APPLICATIONS OVERVIEW

3.1 Phase Imaging

Angular selectivity of acousto-optic Bragg diffraction can be used for physical-level phase imaging. For example, it has been previously shown that differential phase imaging can be obtained with gradient transfer functions of an AOTF (Balakshy and Kostyuk, 2009; Balakshy, 2018).

The confocal AOTF scheme, Fig. 5, can process optical images in dark field mode that enables phase imaging. Coherent phase imaging system is a bright-field light microscope with narrowband object illumination and a confocal hyperspectral imaging system placed at the microscope output optical port (Yushkov et al., 2016). Changing the frequency of ultrasound, one can select the spatial frequency transmitted by the AOTF and therefore to change object visualization mode.

Phase imaging with broadband incoherent illumination requires a system modification since different wavelength of the input light will be efficiently diffracted at different spatial frequencies. When a plane wave passes through a phase object its angular spectrum is broadened because of scattering. Lower spatial frequencies of the optical beam are blocked by a spatial light modulator (SLM) placed

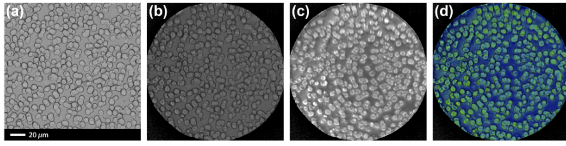


Figure 8: Demonstration of acousto-optic phase imaging: (a) reference image captured with an RGB camera; (b) bright-field spectral image; (c) dark-field phase image; (d) false-color fusion of amplitude-and-phase modulation. Reproduced under Open Access Licence from (Yushkov et al., 2020a), ©2020 OSA.

in a Fourier-conjugated plane of the system (Yushkov et al., 2019a; Yushkov et al., 2020a). Higher spatial frequencies that contain only the scattered light are transmitted to satisfy dark field phase imaging principle. Then the conical beam is spectrally filtered by the AOTF. According to the phase matching surface symmetry, all components of the conical beam are diffracted by the AOTF within the same wavelength window. Matched spectral and spatial filtering results in high resolution wide-field phase imaging.

When the spatial light modulator is switched off, the AOTF operates in a regular bright-field spectral imaging mode. That allows correct calibration of phase imaging and false-color fusion of phase-and-amplitude modulation. An example of phase imaging is shown in Fig. 8.

3.2 Optical Trapping

The phenomenon of optical trapping has been known for four decades (Ashkin, 1992). The range of application of optical traps and tweezers covers many disciplines ranging from microbiology to manipulation of cold atoms. The technology of optical traps is constantly being improved, and recently a need has arisen for dynamical generation of various geometrical configurations of optical traps, which requires advanced methods of laser beam shaping. One of such methods is a noncollinear AOTF based laser beam shaping. The use of several frequencies to feed the AOTF makes it possible to synthesize various radial field distributions and to tune them with sub-10- μ s response time.

Experimental setup of a ring-shaped optical trap is shown in Fig. 9 (Obydenov et al., 2021a; Obydenov et al., 2021b). The optical scheme is a modified Fourier-transform scheme, Fig. 5 (b), with an additional relay lens group between the AOTF and the second Fourier lens. The relay optics performs laser beam magnification and transport from the AOTF to the back focal plane of a microscope objective, which is the second Fourier lens. Thus, the angular aperture of the AOTF was matched with the aperture of

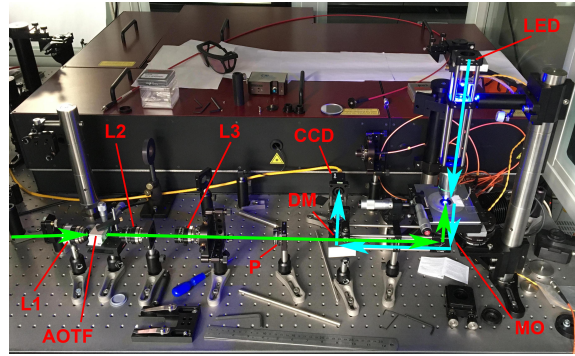


Figure 9: Optical trapping setup based on a noncollinear AOTF: CCD — imaging camera; DM — long-pass dichroic mirror; L1, L2, L3 — lenses; LED — light emitting diode for illumination; MO — microscope objective; P — thin-film polarizer; green arrows — laser beam path at 532 nm; cyan arrows — illumination path at 460 nm.

the objective. Laser radiation with the wavelength of 532 nm was used. Passing through the expander, the laser beam was focused by means of a Fourier lens into the volume of a noncollinear paratellurite AOTF specially optimized and fabricated for this work. The operating frequency of the filter in the wide-aperture diffraction geometry is 132.35 MHz, the bandwidth is 0.24 MHz. The 0th diffraction order at the AOTF output was blocked by a thin-film polarizer. The objective converted the ring-shaped angular spectrum of the beam into spatial intensity distribution, which exposes the sample.

The sample was a suspension of polystyrene microspheres with an average diameter of 10 μ m. The liquid phase of the suspension was deionized water with the addition of a liquid antiseptic and a surfactant to prevent adhesion. The suspension was placed in a special reaction cell made of cover glass. To visualize the sample, we used a transmission Köhler illumination system with a blue diode light source. Passing through the sample, the radiation was collected by an objective and imaged onto on the CCD matrix through a dichroic mirror and a tube lens.

Demonstration of the annular trap operation is shown in Fig. 10. The radius of the trapping ring was controlled by changing the RF signal frequency in the range from 132.4 to 134.0 MHz. A programmable AWG was used for this purpose. Panel (a) shows operation of the trap in a static mode, the radius of the ring being fixed. In this particular example, the microspheres are arranged in a circle with the radius of 80 μ m at $F = 134.0$ MHz. A dynamic trap is shown in panels (b) and (c): the RF signal had sawtooth frequency sweep resulting in generation of a series of convergent or divergent trapping rings. As the result, the microspheres were either aggregated in the center of the trap or repulsed from the center.

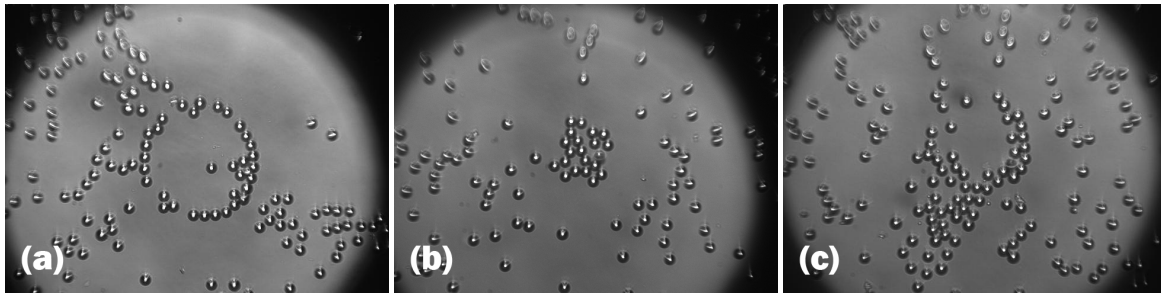


Figure 10: Optical trapping demonstration: (a) static single-ring trap; (b) aggregation of particles by dynamic converging-ring trap; (c) disaggregation of particles by dynamic diverging-ring trap.

4 DISCUSSION

Diffraction efficiency of an AOTF is one of the key performance parameters in applications. According to Eq. 1, for a plane wave component without mismatch $\max H_{ao} = 1$ when $Q = 1$ and $R(k_x, k_y; F) = 0$. In practice, the efficiency can be rather close to 1. Visualization of the 0th diffraction order in Fig. 1 demonstrates overall efficiency above 98% within the whole active aperture of the AOTF. Thus, overall optical losses in the AOTF including Fresnel reflections can be well below 5% for linearly polarized light.

In optical beam shaping applications described in Sec. 3 the beams are spatially filtered by the AOTF, thereby the overall throughput is an integral of the optical beam angular spectrum multiplied by the transfer function H_{ao} . In the case of phase imaging, the optical beam is pre-filtered by the dark-field Fourier-plane filter implemented on the SLM. Therefore angular spectrum of the beam is already matched with the annular AOTF transfer function and the polarization at the SLM output is linear as required for the AOTF. In the case of annular optical trap, a Gaussian input beam was used at the AOTF input. For this reason, lower spatial frequencies of the beam were not used and the diffracted beam intensity was few percent of the input beam even though the diffraction efficiency for phase-matched components of the angular spectrum was above 95%. Optimization of the system throughput by means of refractive flat-top beam shaping (Laskin et al., 2011; Dickey, 2014) before the AOTF will be a plot for future work.

Another potential advancement in AOTF-based laser beam shaping is related to using biaxial crystals. The topology of the transfer function depends on local curvature of the optical wave normal surface in the phase matching region of the k -space (Yushkov and Naumenko, 2021). In a uniaxial crystal, there are only three types on the NPM transfer function, one of them being the annular transfer function discussed in this work. In biaxial crystals, the geometry of the

wave normal surface is more complicated, and other topologies of the transfer function may exist enabling asymmetrical transfer functions, one dimensional tunable k -space filtering, and high-order NPM geometries.

ACKNOWLEDGEMENTS

The author thanks contributions to this work from the Acousto-Optical Research Center team.

The research was supported by the Russian Science Foundation (RSF) under project 21-12-00247.

REFERENCES

- Ashkin, A. (1992). Forces of a single-beam gradient laser trap on a dielectric sphere in the ray optics regime. *Biophys. J.*, 61(2):569–582.
- Balakshy, V. (1984). Acoustooptical cell as the space frequency filter. *Sov. J. Commun. Technol. Electron.*, 29(8):1610–1616.
- Balakshy, V. (2018). Acousto-optic visualization of optical wavefronts. *Appl. Opt.*, 57(10):C56.
- Balakshy, V. and Kostyuk, D. (2009). Acousto-optic image processing. *Appl. Opt.*, 48(7):C24.
- Balakshy, V. and Voloshinov, V. (2005). Acousto-optic image processing in coherent light. *Quantum Electron.*, 35(1):85–90.
- Dickey, F., editor (2014). *Laser Beam Shaping: Theory and Techniques*. CRC Press, Boca Raton, FL, 2nd edition.
- Genchi, L., Bucci, A., Laptinok, S., Giammona, A., and Liberale, C. (2021). Hadamard-transform spectral acquisition with an acousto-optic tunable filter in a broadband stimulated raman scattering microscope. *Opt. Express*, 29(2):2378–2386.
- Goodman, J. (2005). *Introduction to Fourier Optics*. Roberts, New York, 3rd edition.
- Gorevoy, A., Machikhin, A., Martynov, G., and Pozhar, V. (2021). Spatiospectral transformation of noncol-

- limited light beams diffracted by ultrasound in birefringent crystals. *Photonics Res.*, 9(5):687.
- Korablev, O., Belyaev, D., Dobrolenskiy, Y., Trokhimovskiy, A., and Kalinnikov, Y. (2018). Acousto-optic tunable filter spectrometers in space missions. *Appl. Opt.*, 57(10):C103–C119.
- Laskin, A., Shcherbakov, A., Molchanov, V., Laskin, V., and Makarov, O. (2011). Developing the refractive light beam shapers as lossless apodization systems suppressing the side-lobes in Fourier transform optical systems. *Proc. SPIE*, 8011:80110L.
- Lu, G. and Fei, B. (2014). Medical hyperspectral imaging: a review. *J. Biomed. Opt.*, 19(1):010901.
- Obydenov, D., Yushkov, K., and Molchanov, V. (2021a). Acousto-optic annular beam shaping for optical traps and lattices. *Proc. SPIE*, 11926:1192610.
- Obydenov, D., Yushkov, K., and Molchanov, V. (2021b). Ring-shaped optical trap based on acousto-optic tunable spatial filter. *Opt. Lett.*, 46(18):4494.
- Suhre, D., Denes, L., and Gupta, N. (2004). Telecentric confocal optics for aberration correction of acousto-optic tunable filters. *Appl. Opt.*, 43(6):1255–1260.
- Yariv, A. and Yeh, P. (1984). *Optical Waves in Crystals*. Wiley, New York.
- Yushkov, K. (2021). Noncritical acousto-optic Bragg phase matching: Analysis of orthorhombic and monoclinic crystal systems. *Appl. Opt.*, 60(24):7113.
- Yushkov, K., Champagne, J., Kastelik, J.-C., Makarov, O., and Molchanov, V. (2020a). AOTF-based hyperspectral imaging phase microscopy. *Biomed. Opt. Express*, 11(12):7053.
- Yushkov, K., Champagne, J., Kastelik, J.-C., and Molchanov, V. (2019a). Hyperspectral phase imaging with a spatially matched acousto-optical tunable filter. *Proc. SPIE*, 10890:108900V.
- Yushkov, K., Chizhikov, A., Makarov, O., and Molchanov, V. (2020b). Optimization of noncollinear AOTF design for laser beam shaping. *Appl. Opt.*, 59(27):8575.
- Yushkov, K., Gurov, V., and Molchanov, V. (2021a). Engineering of aotf transfer function for phase imaging microscopy and optical trapping. In *European Conferences on Biomedical Optics 2021 (ECBO), OSA Technical Digest*, page ETu3B.5, Munchen, Germany. Optical Society of America.
- Yushkov, K., Makarov, O., and Molchanov, V. (2019b). Novel protocol of hyperspectral data acquisition by means of an acousto-optical tunable filter with synthesized transmission function. *Opt. Lett.*, 44(6):1500.
- Yushkov, K., Molchanov, V., Balakshy, V., and Mantsevich, S. (2018). Acousto-optical transfer functions as applied to laser beam shaping. *Proc. SPIE*, 10744:107440Q.
- Yushkov, K., Molchanov, V., Belousov, P., and Abrosimov, A. (2016). Contrast enhancement in microscopy of human thyroid tumors by means of acousto-optic adaptive spatial filtering. *J. Biomed. Opt.*, 21(1):016003.
- Yushkov, K., Molchanov, V., and Khazanov, E. (2021b). Uncertainty relation in broadband laser pulse shaping. *Phys. Uspekhi*, 64(8):828.
- Yushkov, K. and Naumenko, N. (2021). Optical beam diffraction tensor in birefringent crystals. *J. Opt.*, 60(9):095602.